

# EM-GAN: Fast Stress Analysis for Multi-Segment Interconnect Using Generative Adversarial Networks

Wentian Jin<sup>1</sup>, Sherif Sadiqbacha<sup>1</sup>, Jinwei Zhang<sup>1</sup> and Sheldon X.-D. Tan<sup>1</sup>

**Abstract**—In this paper, we propose a fast transient hydrostatic stress analysis for electromigration (EM) failure assessment for multi-segment interconnects using generative adversarial networks (GANs). Our work leverages the image synthesis feature of GAN-based generative deep neural networks. The stress evaluation of multi-segment interconnects, modeled by partial differential equations, can be viewed as time-varying 2D-images-to-image problem where the input is the multi-segment interconnects topology with current densities and the output is the EM stress distribution in those wire segments at the given aging time. Based on this observation, we train conditional GAN model using the images of many self-generated multi-segment wires and wire current densities and aging time (as conditions) against the COMSOL simulation results. Different hyperparameters of GAN were studied and compared. The proposed algorithm, called *EM-GAN*, can quickly give accurate stress distribution of a general multi-segment wire tree for a given aging time, which is important for full-chip fast EM failure assessment. Our experimental results show that the *EM-GAN* shows 6.6% averaged error compared to COMSOL simulation results with orders of magnitude speedup. It also delivers  $8.3\times$  speedup over state-of-the-art analytic based EM analysis solver.

## I. INTRODUCTION

Electromigration (EM) is a primary long-term reliability concern for copper-based back-end-of-the-line interconnects used in modern semiconductor chips. As predicted by ITRS, EM is projected to only get worse in future technology nodes [1]. This, as with many other reliability effects, is due to the continued trend of feature-size reduction and rapid integration which ultimately affects the critical sizes for the EM failure process. EM-related aging and reliability will become worse for current 7nm and below technologies. As a result, it is crucial to ensure the reliability of the VLSI chips during their projected lifetimes.

Due to its growing importance, considerable recent research has focused on fast EM analysis techniques. It is well accepted that existing Black and Blech-based EM models [2], [3] are overly conservative and can only work for single wire segment [4], [5]. Recently, a number of physics-based EM model and analysis techniques have been proposed [6]–[18]. At the center of those methods is to solve partial differential equation (called Korhonen’s equation) of stress in the confined metal wire segments in a general interconnect tree [19]. Although many numerical approaches such as finite method [12], [13], finite element methods [6], [15] and analytic or semi-analytic solutions [9], [11], [14], [16], [17] were proposed, these methods still suffer the high computing costs or can only apply to some special cases, which hinder this applications for full-chip EM validation and signoff analysis.

On the other hand, deep neural networks (DNN) have propelled an evolution in machine learning fields and redefined many existing applications with new human-level AI capabilities. DNNs such as convolution neural networks (CNN) have recently been applied to many cognitive applications such as visual object recognition, object detection, speech recognition,

natural language understanding, and etc. due to dramatic accuracy improvements in those tasks [20]. Recently, generative adversarial networks (GAN) [21] gained much traction as it can learn features (latent representation) without extensively annotated training data. The representations learned by GANs may be used in a variety of applications, including image synthesis, semantic image editing, style transfer, image super-resolution, and classification. Recently GAN-based methods have been applied for VLSI physical designs such as for layout lithography analysis [22] and sub-resolution assist feature generation [23], for analog layout well generation [24] and for routing congestion estimation [25].

In this work, we propose a fast transient hydrostatic stress analysis technique for EM failure assessment of multi-segment interconnects using GANs. The new contributions are as follows:

1. We propose a fast GAN-based stress analysis solver, called *EM-GAN* for multi-segment interconnect wire tree. We treat the partial differential equation solving process as a time-varying 2D-image-to-image process where the input is the multi-segment interconnects topology with current densities and aging time and the output is the EM stress distribution in those wire segments at the given aging time.
2. We design the architecture and hyper parameters of the *EM-GAN* solver. Different hyper parameters of GAN were studied and compared. We use current densities of wire segment and aging time as the conditions for the conditional GAN. The resulting *EM-GAN* can quickly give accurate stress distribution of any multi-segment wires for a given aging time.
3. Our experimental results show that the *EM-GAN* has 6.6% averaged error compared to COMSOL [26] simulation results with orders of magnitude speedup. It also delivers  $8.3\times$  speedup over recently proposed state-of-the-art analytic based EM analysis solver [17].

## II. PHYSICS-BASED EM MODELING AND ANALYSIS

EM is the process of metal atoms migrating along the direction of the applied electric field in confined metal interconnect wires due to the momentum transfer between the conducting electrons and lattice atoms. Under EM, the aforementioned momentum transfer leads to the buildup of hydrostatic stress in the confined metal wires. When this stress reaches a critical level, the aforementioned migration of atoms is initiated. Over time, this migration leaves behind a depletion of atoms (or void) at the cathode terminal of the wire and an accumulation of atoms (or hillock) at the anode terminal. This eventually leads to failure due to an open or short circuit respectively.

Traditionally, the industry standard model to predicting the time-to-failure (TTF) under EM are based on empirical or statistical models, the most well known of which are Black’s equation [2] and Blech’s limit [3]. However those models have been shown to be overly conservative, applicable only to single wire segment, and therefore lead to unnecessary over-design with large overheads [5]. To mitigate this problem, EM

<sup>1</sup>Wentian Jin, Sherif Sadiqbacha, Jinwei Zhang and Sheldon X.-D. Tan are with the Department of Electrical and Computer Engineering, University of California, Riverside, CA 92521.

modeling starts with the first principles of stress physics in the confined metal wires start to gain many tractions [18]. Such physics-based EM modeling analysis is centering around solving the partial differential equation with blocked terminal boundary conditions for general multi-segment interconnects as shown in Fig. 1.

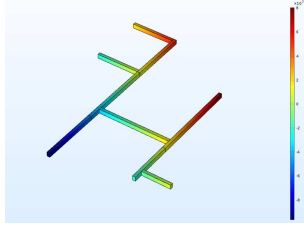


Fig. 1: Multi-segment wire with EM stress distribution

Specifically, we assume that a general interconnect wire has  $n$  nodes, including  $p$  interior junction nodes  $x_r \in \{x_{r1}, x_{r2}, \dots, x_{rp}\}$  and  $q$  block terminals  $x_b \in \{x_{b1}, x_{b2}, \dots, x_{bq}\}$ . Then the Korhonen's PDE [19] for the nucleation phase can be written in following multi-segment format:

$$\begin{aligned} \frac{\partial \sigma_{ij}(x, t)}{\partial t} &= \frac{\partial}{\partial x} \left[ \kappa_{ij} \left( \frac{\partial \sigma_{ij}(x, t)}{\partial x} + G_{ij} \right) \right], t > 0; \\ BC : \sigma_{ij_1}(x_i, t) &= \sigma_{ij_2}(x_i, t), t > 0; \\ BC : \sum_{ij} w_{ij} \kappa_{ij} \left( \frac{\partial \sigma_{ij}(x, t)}{\partial x} \right) \Big|_{x=x_r} &+ G_{ij} \cdot n_r = 0, t > 0 \\ BC : \kappa_{ij} \left( \frac{\partial \sigma_{ij}(x, t)}{\partial x} \right) \Big|_{x=x_b} &+ G_{ij} = 0, t > 0; \\ IC : \sigma_{ij}(x, 0) &= \sigma_{ij,T} \end{aligned} \quad (1)$$

where  $\sigma(x, t)$  is the hydrostatic stress for branch  $ij$  from nodes  $i$  and  $j$ ,  $n_r$  represents the unit inward normal direction of the interior junction node  $r$  on branch  $ij$ , the value of which is  $+1$  for right direction and  $-1$  for left direction of branch with assumption of  $x_i < x_j$ ,  $G = \frac{Eq*}{\Omega}$  is the EM driving force,  $w$  is the width of the branch, and  $\kappa = D_a B \Omega / k_B T$  is the diffusivity of stress.  $E$  is the electric field,  $q*$  is the effective charge.  $D_a = D_0 \exp(-\frac{E_a}{k_B T})$ , which is the effective atomic diffusion coefficient.  $D_0$  is the pre-exponential factor,  $B$  is the effective bulk elasticity modulus,  $\Omega$  is the atomic lattice volume,  $k_B$  is the Boltzmann's constant,  $T$  is the absolute temperature,  $E_a$  is the EM activation energy.  $\sigma_T$  is the initial thermal-induced residual stress in each wire segment.

In general, numerical approaches such as finite difference, finite element based approaches are required to solve the PDE in (1), which are expensive and time consuming. The recently proposed semi-analytic solutions can still be expensive as the eigenvalues have to be computed by numerical approaches [14], [17].

On the other hand, we can view the PDE solving process for a multi-segment wire shown in Fig. 1 as image synthesis process, in which the deep neural networks (DNN) can automatically extract features reflecting the physics-law of stress evolution in the confined metal wire, then we can use the DNN network to map the input images of interconnect wires with stressing current or voltages to the stress distributions of wire segment for any given aging time.

### III. DATA PREPARATION

For machine learning based approaches, one crucial aspect is sufficient training data. For our GAN-based EM stress estimation, it also requires a large amount of interconnect topologies with various current densities and corresponding ground truth EM stress distribution data from which the model can learn the transformation scheme in between. In what follows, we present the training data required by our model and the method to collect them. Some necessary pre-processing methods performed on the training set prior to feeding them to the model will also be discussed.

To achieve the abundance in the training set, we randomly generated 2500 different topologies of multi-segment interconnects with various wire width, number of branches and current densities. The raw topology and the current density data are separately stored in numerical format. They are given to the COMSOL, which is a finite element method (FEM) solver, as input and the resulting EM stress distributions at 1 to 10 discrete aging years are saved as ground truth. As mentioned in Section I, to leverage the GAN model, we view this solving process as an image-to-image problem. Both interconnects topology and current information can be synthesized into a 2D-image (called *design* in this work) shown in Fig. 2a. The image actually has only one channel instead of red-green-blue (RGB) channels and the color in Fig. 2a is only for illustration purpose. Every current density value is filled into its position in the topology and zeroes are padded to all positions without an interconnect. To make it easier for a neural network to handle, we fixed the dimensions of each design to  $256 \times 256 \mu\text{m}^2$  and make each pixel represent  $1 \mu\text{m}$ . Such setting does not restrict our work to only small dimensions as in real applications, bulk interconnect system may be divided into small pieces with partitioning algorithms for parallel simulation. The ground truth EM stress distribution is also synthesized into single-channel images with pixels filled with stress values, as shown in Fig. 2b. Our training set contains 25000 samples where each sample is a (input design image, target EM stress image) pair.

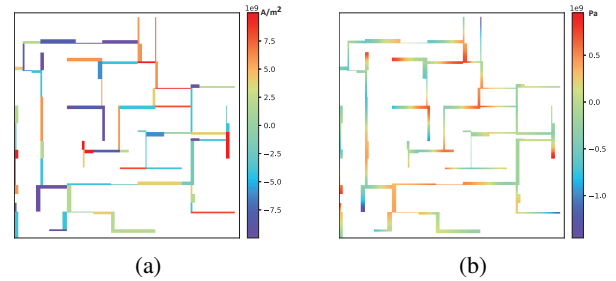


Fig. 2: Illustration of a random training data: (a) Interconnect topology with current density (b) EM stress distribution at 10th aging year.

As the pixels in our images are not RGB colors but real current density or EM stress values instead, they can range drastically from magnitude of  $-10^9$  to  $10^9$  in which minus denotes the current directions toward left and down sides. Such a large numerical range is not suitable for neural networks and requires to be scaled down. In this work, we rescaled all samples in the training set to mean value of 0 and standard deviation of 1 using data standardization method. It squeezes all data to the range of -7 to 7 and most of which are around zero.

#### IV. CGAN-BASED CURRENT DENSITY TO EM STRESS ESTIMATION

##### A. GANs and CGANs

The GAN is a neural network model that is used in unsupervised machine learning tasks and was created by Ian Goodfellow [27]. A traditional GAN is composed of two separate deep neural networks, one is generator  $G$  and the other is discriminator  $D$ .  $G$  is trained to generate “real-like” output that resembles the data in the training set while, on the contrary,  $D$  is trained as a judge to distinguish between the real and generated data. The generator in a conventional GAN takes random noise vector  $z$  as input and transforms it into the output  $G(z)$ . Both real and generated data are alternatively given to the discriminator which is typically a deep binary classifier and output a “score”. The input data are classified as “real” or “fake” based on the score which also serves as part of the loss function. It is used to train both  $G$  and  $D$  through back propagation. The training processes of both networks are performed simultaneously in an alternative way to ensure neither of them is lagging too much behind the other until an equilibrium is reached.

The conditional GAN is a GAN working in the conditional setting and learns a conditional generative model. Unlike the conventional GAN, the input of the generator is a combination of both condition vector  $x$  and random noise vector  $z$  and the output is denoted as  $G(x, z)$ . The main difference compared to GAN is that both  $G$  and  $D$  in CGAN are conditioned on the vector  $x$ . CGAN has been shown working perfectly in image-to-image translation works where the input image is seen as the condition and constrains the image generation process. In our context, the generated EM stress distribution is conditioned on the input current density and given aging time according to physics-law of stress evolution, which is highly suitable for the CGAN model.

The training of GAN is quite challenging given the fact that such process is a minimax game between two separate neural networks. The objective function of either generator or discriminator is influenced not only by itself but also by its opponent. As a result, when the discriminator is much better trained than the generator, the gradient vanishes to zero and the generator is unable to get useful learning information from it. To mitigate this convergence problem, Wasserstein GAN(WGAN) was introduced by Martin Arjovsky in [28]. It replaces the conventional JS-Divergence with Wasserstein distance as the measurement of the difference between real and generated data which solves the vanishing gradient problem. In this work, we employ the Wasserstein distance in the loss functions to help the convergence. It also mitigates the collapse mode problem to some extent and ensures the diversity of the generated data.

##### B. EM-GAN Architecture

To implicitly learn the distribution of the current density image and map it to the corresponding real-like EM stress image, we use a CGAN as backbone for our model shown in Fig. 3. The generator takes the current density image  $img_{cur} \in \mathbb{R}^{256 \times 256 \times 1}$  and the aging years  $t \in \mathbb{R}$  as input.  $t$  is expanded into  $\mathbb{R}^{256 \times 256 \times 1}$  by channel-wise duplication, such that  $img_{cur}$  and  $t$  can be concatenated depth-wise. The resulting input  $x$  given to the generator is a  $256 \times 256 \times 2$  image with all entries normalized as described in Section III. We employ an encoder-decoder architecture as our generator which is widely used in image-to-image applications. In such a network, the input is downsampled through a series of convolutional layers until a bottleneck layer, at which the latent

features are extracted and then reversely upsampled through transposed convolutional layers. All information is supposed to be passed through this bottleneck layer, which is not necessary, as much low-level information is shared between the input and output. In our work, both input and output images share the same topology of interconnect layout. To bypass the bottleneck layer and shuttle such information directly across the network, we add skip connections between the encoder and the decoder. Such architecture greatly helps to improve the result accuracy which is discussed in detail in Section V-C.

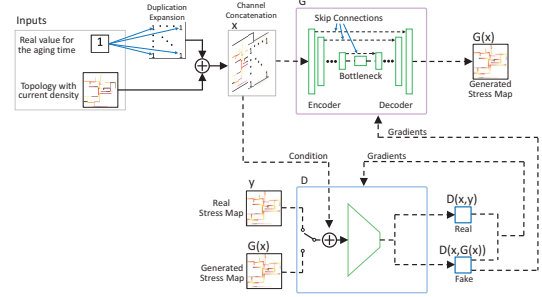


Fig. 3: EM-GAN framework for stress estimation

The output of the generator is denoted as  $G(x)$ . Either the generated  $G(x)$  or the real EM stress image  $y$  is fed into the discriminator  $D$  alternatively together with its corresponding current density and aging time  $x$  as the condition input. The output of the discriminator is denoted as  $D(G(x), x)$  or  $D(y, x)$  depending on which EM stress image, generated or real, was inputted.

The key idea of the proposed EM-GAN model is to get the generator learn the mapping method from the distribution of current density and aging year to that of the EM stress image in the training set. Such transformation is achieved by progressively training the generator according to the gradients back propagated from the loss based on the output of the discriminator. The generator and the discriminator are trained simultaneously but based on separate loss functions. The training goal of the discriminator is to minimize  $D(G(x), x)$  and maximize  $D(y, x)$ , which means higher scores should be given to the real EM stress images than the generated ones. This training objective can be expressed mathematically as

$$\max_D \{ \mathbb{E}_{x,y} [D(y, x)] - \mathbb{E}_x [D(G(x), x)] - \lambda_{gp} \mathbb{E}_{\hat{x}} [(\|\nabla_{\hat{x}} D(\hat{x}, x)\|_2 - 1)^2] \} \quad (2)$$

$\mathbb{E}_{x,y}$  and  $\mathbb{E}_x$  are the expectations over the distributions of  $x$  and  $y$ . The last term in (2) is the gradient penalty which is adopted from WGAN-GP [28].  $\hat{x}$  is interpolation between the generated EM stress image and its ground truth. The hyperparameter  $\lambda_{gp}$  is the weight of the gradient penalty which maintains the 1-Lipschitz continuity of the discriminator.

On the contrary, the training objective for the generator is to deceive the discriminator and get higher scores for its generated EM stress images. As the generator has no influence on the scores of the real images, term  $D(y, x)$  is discarded in its objective function. We also add a L2-norm to the loss of the generator, as is shown in (3), to further improve the objective function according to [29].  $\lambda_{L2}$  controls the strength of the L2-norm distance penalty on the loss of generator.

$$\min_G \{ \mathbb{E}_x [-D(G(x), x)] + \lambda_{L2} \cdot \mathbb{E}_{x,y} [\|y - G(x)\|_2] \} \quad (3)$$

In both (2) and (3), we use the Wasserstein distance as the measurement of the difference between the real and the

generated EM stress image distribution to take advantage of higher stability and convergence possibility. The detailed architectures of the generator and the discriminator in our proposed EM-GAN are illustrated in Fig. 4.

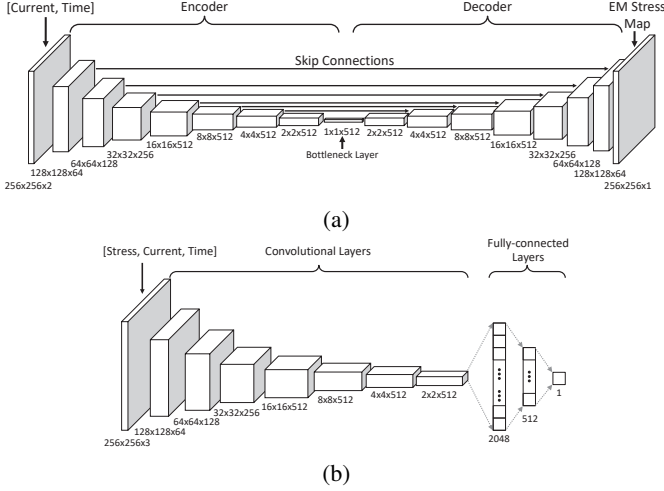


Fig. 4: The architecture of the neural networks in the proposed EM-GAN: (a) generator (b) discriminator.

## V. EXPERIMENTAL RESULTS AND DISCUSSIONS

In this section, we present the experimental results showing both the accuracy and speed of our proposed EM-GAN model for time dependent EM stress estimation.

All of our model is implemented in Python basing on TensorFlow(1.14.0) library [30] which is an open-source machine learning platform. To train the GAN model, a dataset containing 25000 pairs of (Current density image with topology and aging time, EM stress image) samples is used. The samples were derived from 2500 different designs of multi-segment interconnects. For each design, we collect the EM stress maps simulated by COMSOL at 10 discrete aging time instants(1 to 10 years). Random selection of 15% designs is set aside for testing purpose and the remaining 85% form the training set. During the training phase, all samples are randomly permuted at the beginning of every epoch.

We run the training for 15 epochs on a Linux server with 2 Xeon E5-2698v2 2.3GHz processors and Nvidia Titan X GPU. The cudnn library is used to accelerate the training process on GPU. To employ mini-batch stochastic gradient descent(SGD), we set the batch size to 8 and solve it with the RMSProp optimizer. The learning rate of the optimizer is 0.0001, where the decay, momentum and epsilon parameters are set to 0.9, 0 and  $10^{-10}$  respectively. The weight of the L2-norm distance  $\lambda_{L2}$  is set to 100.

### A. Accuracy of EM Stress Map Estimation

Once the EM-GAN model is trained, the generator is preserved and serve as the generative model. It can take any multi-segment interconnects design as input and estimate the EM stress map at a given aging year. To evaluate the estimation error against the ground truth, we employ the root-mean-square error(RMSE) and the normalized RMSE(NRMSE) given in (4) and (5) as the Metrics.

$$RMSE = \sqrt{\frac{\sum_{(x,y) \in S} [\sigma(x,y) - \sigma'(x,y)]^2}{|S|}} \quad (4)$$

$$NRMSE = \frac{RMSE}{\sigma_{max} - \sigma_{min}} \quad (5)$$

where  $\sigma$  and  $\sigma'$  are the real and generated EM stress map respectively.  $S$  is the set containing all positions with an interconnect and  $|S|$  denotes the number of pixels in  $S$ .  $\sigma_{max}$  and  $\sigma_{min}$  denote the maximum and minimum stresses in the ground truth EM stress image.

We evaluate our trained EM-GAN model on the testing set which was set aside during the training phase. The designs in the testing set were randomly generated in the same way as the training set was produced. The random generation process guarantees that there is no overlap of either topology or current densities between these two datasets. It means that all designs used for evaluation are unseen and absolutely new to the model. This testing set makes our work more practically meaningful, as in real applications, it is merely possible that the design given to the model is identical to any design used for training. Otherwise, it will make the model more of a memory system leading to a low ability of generalization.

A total number of 375 different designs are tested and for each of them, 10 EM stress images at 1 to 10 discrete aging years are generated by our EM-GAN model. Comparing all 3750 generated EM stress images with the ground truth, EM-GAN achieves an average estimation RMSE of 0.13 GPa and NRMSE of 6.6%. Considering the large range the values of typical EM stress vary in, usually several GPa, such accuracy is beyond enough for EM failure assessment such as critical wire identification. We randomly pick two testing designs and compare the EM stress estimation at 1, 4, 7 and 10 aging years with the ground truth COMSOL simulation results in Fig. 7. The unit of the current density is  $A/m^2$  and EM stress is shown in  $Pa$ .

### B. Speed of Inference

In what follows, we provide a comparison of speed between our EM-GAN and the state-of-the-art work [17] on EM stress analysis. We set up the problem as a large multi-segment interconnects design that can be divided into 528 smaller designs with same dimensions of  $256 \times 256 \mu m^2$ . We randomly pulled the small designs from both training and testing set. The number of branches in each design ranges from 5 to 79. Both our EM-GAN model and the [17] method were tested to generate the EM stress estimation at 10th aging year. The experiments were performed on the same server and the accumulating time cost on all designs are plotted in Fig. 5.

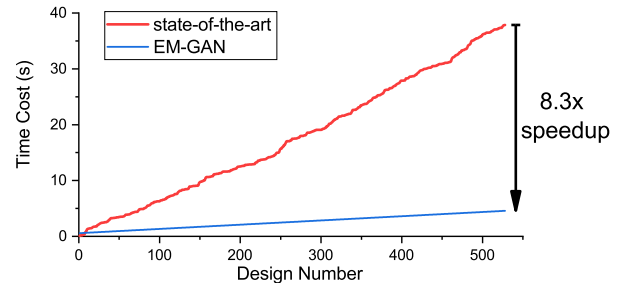


Fig. 5: Comparison of EM stress estimation speed between state-of-the-art and EM-GAN.

The total time cost on the 528 small designs are 37.86s and 4.58s for [17] and EM-GAN respectively. The EM-GAN demonstrates  $8.3 \times$  speedup over [17]. For [17], the time cost on the estimation of a single design varies from 0.49s to 0.003s



depending on the number of branches in the design. For EM-GAN, there is no difference between designs with different branches, and the inference speed is steadily around 8ms per design throughout the experiment. The time cost of EM-GAN is invariant to interconnect branches, which makes it much more suitable for larger scale designs and leads to a better scalability.

### C. Analysis of Loss and Skip Connections

As described in Section IV-B, our EM-GAN model employs skip connections in the generator to bypass the bottleneck layer in conveying the topology information from the encoder to the decoder. We also applied L2-norm distance in the loss function of the generator to enhance its performance. To analyze whether and how these modifications are helpful to our application, we trained two other modified models with similar structures as the proposed EM-GAN except that one has no skip connection and the other discarded the L2-norm in the objective function.

Both modified models are trained until convergence and tested against the same training and testing set used by the EM-GAN. Both models achieved worse errors on the testing set with NRMSE of 15.2% for the model without skip connection and 8.4% for the one without L2-norm. Also, our proposed EM-GAN demonstrates a smaller mean and standard deviation in errors than the other two modified models, as shown in Table I. In Fig. 6, we show the comparison between the inference results generated by these models and the ground truth using one randomly selected design from the testing set. Two models with skip connections outperform the other one by a significant margin. This can be accounted by the fact that the bottleneck layer handles both structure and current information in conventional encoder-decoder model. However, when skip connections are added, topology information is directly passed from encoder to decoder and only current density information is left to pass through the bottleneck. It greatly increases the bandwidth of the information flow within the model and helps increase the overall accuracy.

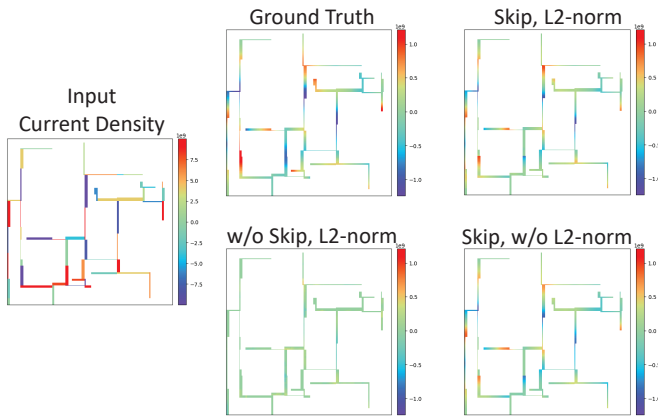


Fig. 6: Comparison of inference results between different models and the ground truth.

The model without L2-norm distance in its objective function degenerates the NRMSE by a small margin from 6.6% to 8.4%. This can be verified in Fig. 6 that both EM stress images generated by the model with or without L2-norm are similar to each other. However, the model with L2-norm has a much faster converging speed in the training process and is

TABLE I: Statistics of NRMSE for EM-GAN and modified models on testing set.

Metrics	EM-GAN (Skip, L2-norm)	w/o Skip, L2-norm	Skip, w/o L2-norm
Mean	6.6%	15.2%	8.4%
Standard Deviation	1.2%	2.1%	2.1%
Max	12.9%	24.6%	18.4%
Min	3.1%	9.8%	3.8%

always closer to the ground truth than the one without L2-norm. It is a reasonable result that the L2-norm helps the model as a prior knowledge. At the very beginning of training process, both discriminator and generator are not well trained and the discriminator is not able to provide useful guidance to the generator. This is where L2-norm can complement the discriminator and provide the generator with a meaningful learning direction. In our experiment, adding the L2-norm accelerates the convergence speed by  $2\times$  and also leads to a better inference accuracy.

## VI. CONCLUSION

In this paper, we have proposed a GAN-based fast transient hydrostatic stress analysis for EM failure assessment for multi-segment interconnects. In our approach, we treat this traditional numerical PDE solving problem as time-varying 2D-image-to-image problem where the input is the multi-segment interconnects topology with current densities and the output is the EM stress distribution in those wire segments at the given aging time. We randomly generated the training set and trained the model with the COMSOL simulation results. Different hyperparameters of GAN were studied and compared. After the training process, the proposed EM-GAN model is tested against 375 unseen multi-segment interconnects designs and achieved high accuracy with an average error of 6.6%. It also showed  $8.3\times$  speedup over recently proposed state of the art analytic based EM analysis solver.

## REFERENCES

- [1] International technology roadmap for semiconductors (ITRS), 2015. <http://www.itrs2.net/itrs-reports.html>.
- [2] J. R. Black. Electromigration-A Brief Survey and Some Recent Results. *IEEE Trans. on Electron Devices*, 16(4):338–347, 1969.
- [3] I. A. Blech. Electromigration in thin aluminum films on titanium nitride. *Journal of Applied Physics*, 47(4):1203–1208, 1976.
- [4] M Hauschildt, C Henneßthal, G Talut, O Aubel, M Gall, K B Yeap, and E Zschech. Electromigration Early Failure Void Nucleation and Growth Phenomena in Cu And Cu(Mn) Interconnects. In *IEEE Int. Reliability Physics Symposium (IRPS)*, pages 2C.1.1–2C.1.6, 2013.
- [5] V. Sukharev. Beyond Black’s Equation: Full-Chip EM/SM Assessment in 3D IC Stack. *Microelectronic Engineering*, 120:99–105, 2014.
- [6] RL De Orio, Hajdin Ceric, and Siegfried Selberherr. Physically based models of electromigration: From black’s equation to modern tcad models. *Microelectronics Reliability*, 50(6):775–789, 2010.
- [7] X. Huang, A. Kteyan, S. X.-D. Tan, and V. Sukharev. Physics-based electromigration models and full-chip assessment for power grid networks. *IEEE Trans. on Computer-Aided Design of Integrated Circuits and Systems*, 35(11):1848–1861, Nov. 2016.
- [8] Valeriy Sukharev, Armen Kteyan, and Xin Huang. Postvoiding stress evolution in confined metal lines. *IEEE Transactions on Device and Materials Reliability*, 16(1):50–60, 2016.
- [9] H. Chen, S. X.-D. Tan, X. Huang, T. Kim, and V. Sukharev. Analytical modeling and characterization of electromigration effects for multibranch interconnect trees. *IEEE Trans. on Computer-Aided Design of Integrated Circuits and Systems*, 35(11):1811–1824, 2016.
- [10] V. Mishra and S. S. Sapatnekar. Predicting Electromigration Mortality Under Temperature and Product Lifetime Specifications. In *Proc. Design Automation Conf. (DAC)*, pages 1–6, Jun. 2016.

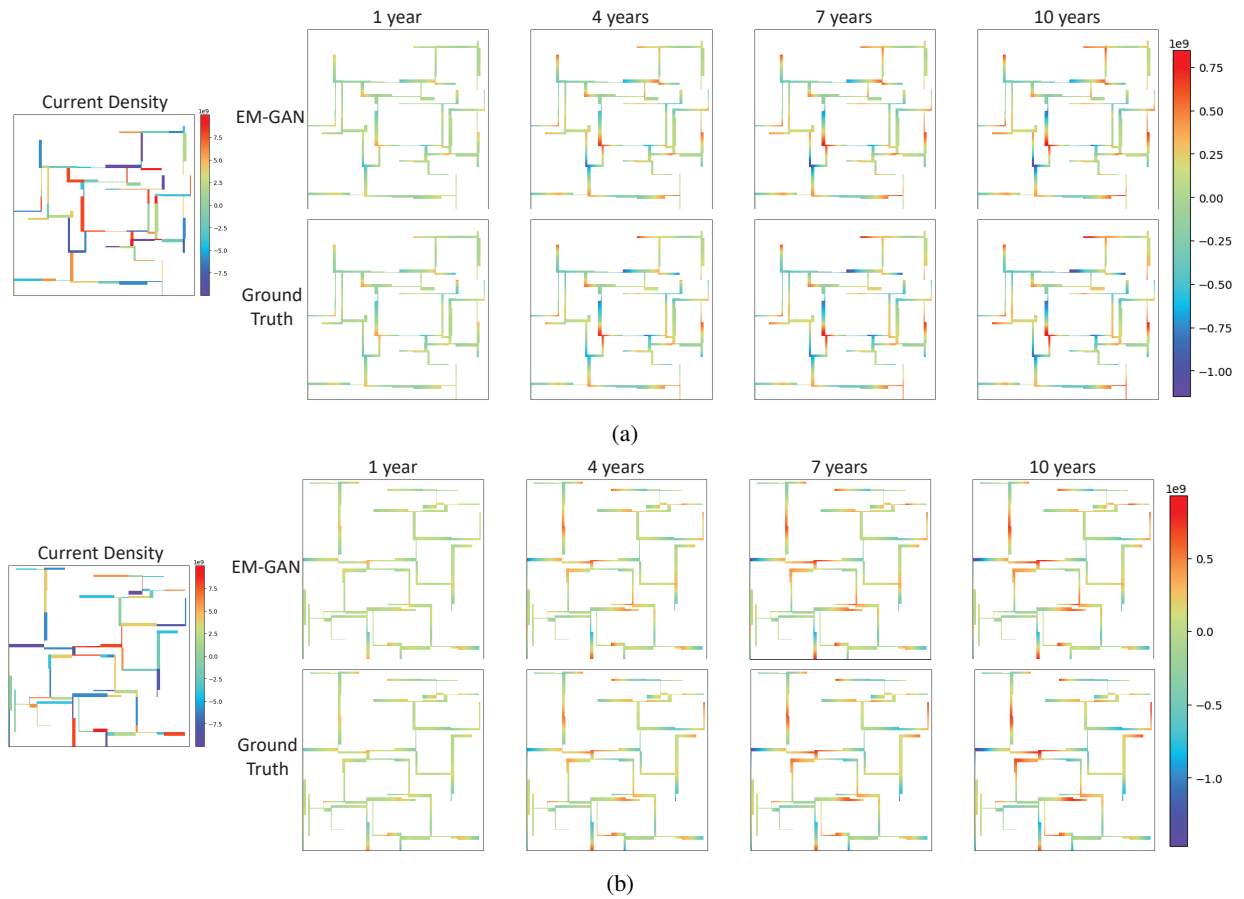


Fig. 7: Comparing the ground truth EM stress distribution with EM-GAN generated ones using two different designs.

- [11] H.-B. Chen, S. X.-D. Tan, J. Peng, T. Kim, and J. Chen. Analytical modeling of electromigration failure for vlsi interconnect tree considering temperature and segment length effects. *IEEE Transaction on Device and Materials Reliability (T-DMR)*, 17(4):653–666, 2017.
- [12] S. Chatterjee, V. Sukharev, and F. N. Najm. Power grid electromigration checking using physics-based models. *IEEE Transactions on Computer-Aided Design of Integrated Circuits and Systems*, 37(7):1317–1330, July 2018.
- [13] C. Cook, Z. Sun, E. Demircan, M. D. Shroff, and S. X.-D. Tan. Fast electromigration stress evolution analysis for interconnect trees using krylov subspace method. *IEEE Trans. on Very Large Scale Integration (VLSI) Systems*, 26(5):969–980, May 2018.
- [14] S. Wang, Z. Sun, Y. Cheng, S. X.-D. Tan, and M. Tahoori. Leveraging recovery effect to reduce electromigration degradation in power/ground TSV. In *Proc. Int. Conf. on Computer Aided Design (ICCAD)*, pages 811–818. IEEE, Nov. 2017.
- [15] H. Zhao and S. X.-D. Tan. Postvoiding fem analysis for electromigration failure characterization. *IEEE Trans. on Very Large Scale Integration (VLSI) Systems*, 26(11):2483–2493, Nov. 2018.
- [16] Ali Abbasinasab and Malgorzata Marek-Sadowska. RAIN: A tool for reliability assessment of interconnect networks—physics to software. In *Proc. Design Automation Conf. (DAC)*, pages 133:1–133:6, New York, NY, USA, 2018. ACM.
- [17] L. Chen, S. X.-D. Tan, Z. Sun, S. Peng, M. Tang, and J. Mao. Fast analytic electromigration analysis for general multisegment interconnect wires. *IEEE Transactions on Very Large Scale Integration (VLSI) Systems*, pages 1–12, 2019.
- [18] Sheldon X.-D. Tan, Mehdi Tahoori, Taeyoung Kim, Shengcheng Wang, Zeyu Sun, and Saman Kiammehr. *VLSI Systems Long-Term Reliability – Modeling, Simulation and Optimization*. Springer Publishing, 2019.
- [19] M. A. Korhonen, P. Bořgesen, K. N. Tu, and C.-Y. Li. Stress evolution due to electromigration in confined metal lines. *Journal of Applied Physics*, 73(8):3790–3799, 1993.
- [20] Yann LeCun, Yoshua Bengio, and Geoffrey Hinton. Deep learning. *Nature*, 521(7553):436–444, May 2015.
- [21] Ian Goodfellow, Yoshua Bengio, and Aaron Courville. *Deep learning*. MIT press, 2016.
- [22] Wei Ye, Mohamed Baker Alawieh, Yibo Lin, and David Z. Pan. Lithogan: End-to-end lithography modeling with generative adversarial networks. In *Proceedings of the 56th Annual Design Automation Conference 2019, DAC '19*, pages 107:1–107:6, New York, NY, USA, 2019. ACM.
- [23] Mohamed Baker Alawieh, Yibo Lin, Zaiwei Zhang, Meng Li, Qixing Huang, and David Z. Pan. Gan-sraf: Sub-resolution assist feature generation using conditional generative adversarial networks. In *Proceedings of the 56th Annual Design Automation Conference 2019, DAC '19*, pages 149:1–149:6, New York, NY, USA, 2019. ACM.
- [24] Biying Xu, Yibo Lin, Xiyuan Tang, Shaolan Li, Linxiao Shen, Nan Sun, and David Z. Pan. Wellgan: Generative-adversarial-network-guided well generation for analog/mixed-signal circuit layout. In *Proceedings of the 56th Annual Design Automation Conference 2019, DAC '19*, pages 66:1–66:6, New York, NY, USA, 2019. ACM.
- [25] Cunxi Yu and Zhiru Zhang. Painting on placement: Forecasting routing congestion using conditional generative adversarial nets. In *Proceedings of the 56th Annual Design Automation Conference 2019, DAC '19*, pages 219:1–219:6, New York, NY, USA, 2019. ACM.
- [26] Comsol multiphysics. <https://www.comsol.com/> [Oct. 16, 2013].
- [27] Ian Goodfellow, Jean Pouget-Abadie, Mehdi Mirza, Bing Xu, David Warde-Farley, Sherjil Ozair, Aaron Courville, and Yoshua Bengio. Generative adversarial nets. In Z. Ghahramani, M. Welling, C. Cortes, N. D. Lawrence, and K. Q. Weinberger, editors, *Advances in Neural Information Processing Systems 27*, pages 2672–2680. Curran Associates, Inc., 2014.
- [28] Martin Arjovsky, Soumith Chintala, and Léon Bottou. Wasserstein GAN. *arXiv e-prints*, page arXiv:1701.07875, Jan 2017.
- [29] Phillip Isola, Jun-Yan Zhu, Tinghui Zhou, and Alexei A. Efros. Image-to-image translation with conditional adversarial networks. In *The IEEE Conference on Computer Vision and Pattern Recognition (CVPR)*, July 2017.
- [30] Martín Abadi, Paul Barham, Jianmin Chen, Zhifeng Chen, Andy Davis, Jeffrey Dean, Matthieu Devin, Sanjay Ghemawat, Geoffrey Irving, Michael Isard, Manjunath Kudlur, Josh Levenberg, Rajat Monga, Sherry Moore, Derek G. Murray, Benoit Steiner, Paul Tucker, Vijay Vasudevan, Pete Warden, Martin Wicke, Yuan Yu, and Xiaoqiang Zheng. Tensorflow: A system for large-scale machine learning. In *12th USENIX Symposium on Operating Systems Design and Implementation (OSDI 16)*, pages 265–283, Savannah, GA, November 2016. USENIX Association.